Titan's corona: The contribution of exothermic chemistry

V. De La Haye [a], J.H. Waite Jr. [a,*], T.E. Cravens [b], A.F. Nagy [c], R.E. Johnson [d], S. Lebonnois [e], I.P. Robertson [b]

[a] *Southwest Research Institute, San Antonio, TX 78228, USA*
[b] *Department of Physics and Astronomy, University of Kansas, Lawrence, KS 66045, USA*
[c] *AOSS Department, University of Michigan, Ann Arbor, MI 48109, USA*
[d] *Astronomy Department, University of Virginia, Charlottesville, VA 22904, USA*
[e] *Laboratoire de Météorologie Dynamique, Jussieu, 75252 Paris, France*

Abstract

The contribution of exothermic ion and neutral chemistry to Titan's corona is studied. The production rates for fast neutrals N_2, CH_4, H, H_2, $^3CH_2$, CH_3, C_2H_4, C_2H_5, C_2H_6, $N(^4S)$, NH, and HCN are determined using a coupled ion and neutral model of Titan's upper atmosphere. After production, the formation of the suprathermal particles is modeled using a two-stream simulation, as they travel simultaneously through a thermal mixture of N_2, CH_4, and H_2. The resulting suprathermal fluxes, hot density profiles, and energy distributions are compared to the N_2 and CH_4 INMS exospheric data presented in [De La Haye, V., Waite Jr., J.H., Johnson, R.E., Yelle, R.V., Cravens, T.E., Luhmann, J.G., Kasprzak, W.T., Gell, D.A., Magee, B., Leblanc, F., Michael, M., Jurac, S., Robertson, I.P., 2007. J. Geophys. Res., doi:10.1029/2006JA012222, in press], and are found insufficient for producing the suprathermal populations measured. Global losses of nitrogen atoms and carbon atoms in all forms due to exothermic chemistry are estimated to be 8.3×10^{24} $N\,s^{-1}$ and 7.2×10^{24} $C\,s^{-1}$.
© 2007 Elsevier Inc. All rights reserved.

Keywords: Titan, atmospheres; Atmospheres chemistry; Photochemistry; Collisional physics

1. Introduction

Suprathermal mechanisms play an important role in heating Titan's upper atmosphere as well as in regulating the escape flux, which is a source of neutral atoms and molecules in Saturn's magnetosphere. Solar radiation and energetic electrons and ions from Saturn's magnetosphere constitute the two main sources of energy for Titan's upper atmosphere. The energy carried by solar photons or magnetospheric electrons penetrating into Titan's atmosphere is absorbed by the main atmospheric constituents, nitrogen and methane. Dissociations and ionizations of N_2 and CH_4 follow, initiating a cascade of exothermic neutral–neutral and ion–neutral reactions, leading to the formation of complex hydrocarbon and nitrile species. These exothermic reactions produce suprathermal particles, which can heat the thermosphere, or penetrate the exosphere and either

escape or contribute to Titan's corona. The ions incident into Titan's upper atmosphere originate either from Saturn's magnetosphere or from local pick-up ions, i.e., neutrals in Titan's corona that are ionized and re-impact the exobase. Those ions penetrating into Titan's neutral atmosphere lose their energy via momentum transfer collision producing energetic atmospheric neutrals. A fraction of these neutrals travel upward and either follow ballistic trajectories and contribute to Titan's corona, or have sufficient energy to escape from Titan's gravitational field, a mechanism referred to as atmospheric sputtering.

Recent observations by INMS onboard Cassini, comparing atmospheric and exospheric data, showed the presence of significant N_2 and CH_4 suprathermal populations in Titan's upper atmosphere (De La Haye et al., 2007). From the analysis of the data recorded during the first close flybys of Titan, T_A, T_B, and T_5, the suprathermal density and energy density at the exobase were estimated to be $4.4 \pm 5.1 \times 10^5$ cm^{-3} and $1.1 \pm 0.9 \times 10^2$ $eV\,cm^{-3}\,s^{-1}$ for the hot nitrogen molecules, and $1.1 \pm 0.9 \times 10^5$ cm^{-3} and $3.9 \pm 3.5 \times 10^1$ $eV\,cm^{-3}\,s^{-1}$ for

---

the hot methane molecules. No suprathermal population was detected in the ingress-T_5 data, although the temperature at the exobase was highest for this pass. These observations confirmed the importance and the spatial complexity of the heating mechanisms taking place in Titan's upper atmosphere, probably involving interactions with Saturn's magnetosphere.

The production of non-thermal neutrals directly induced by energetic particles or photons penetrating into Titan's upper atmosphere have been studied by several groups. The production of hot N atoms through dissociation and dissociative ionization of molecular nitrogen by solar UV radiation, photoelectrons, and magnetospheric electrons were described in Lammer and Bauer (1991), Strobel et al. (1991), Gan et al. (1992), Shematovich (1998). And the production of hot N and N_2 particles through atmospheric sputtering by energetic magnetospheric ions (H^+ and N^+), pick up ions (N_2^+, $C_2H_5^+$), or solar wind protons were described in Lammer and Bauer (1993), Shematovich et al. (2001), Shematovich et al. (2003), Michael et al. (2005), Michael and Johnson (2005).

The complex chemistry involving neutrals and ions in Titan's upper atmosphere represents a significant source of energy, and is also likely to constitute an important source of non-thermal neutrals. Cravens et al. (1997) examined the production of 19 non-thermal neutrals involved in 47 chemical processes. They calculated the hot particles' production rates and heating using the ionospheric model of Keller et al. (1992), and found a global loss of nitrogen and carbon atoms in all forms of 2.5×10^{25} and $1.7-4 \times 10^{25}$ s^{-1}, respectively. In Cravens et al. (1997), ion–neutral and dissociative electron recombination reactions were taken into account as sources of suprathermal neutrals. Neutral–neutral reactions, however, were not considered. In addition, they integrated the production rate profiles between the exobase and 2500 km to estimate the escape rates, but suggested that calculating the distribution function, including collisions with the background neutrals, would provide more accurate results.

In the present study, a two stream model is constructed to model the fate of 12 suprathermal particles (N_2, CH_4, H, H_2, $^3CH_2$, CH_3, C_2H_4, C_2H_5, C_2H_6, N(^{4}S), NH, and HCN) traveling through a background mixture of cold N_2, CH_4, and H_2, the three major species in Titan's upper atmosphere. A coupled ion and neutral model of Titan's upper atmosphere is used to calculate the production rates of the hot particles between 600 and 1450 km, the altitude of the exobase as estimated in De La Haye et al. (2007). The production rate profiles, suprathermal density profiles, and energy distributions are calculated and compared to the INMS exospheric data presented in De La Haye et al. (2007).

2. The two stream model

The present two stream model is built on the principles described in Nagy and Cravens (1981, 1988). The hot particles are assumed to be produced solely through chemical reactions, using production rates determined from the coupled ion and neutral model of Titan's upper atmosphere mentioned in the following section. The energy loss of the

suprathermal particles is considered to occur solely via collisions with the cold ambient neutral gas. The possibility of energy gain for the suprathermal particles through mutual collisions is neglected, but events such as a cold target particle becoming suprathermal after a collision are taken into account. Considering the low energies that are dealt with, inelastic processes are neglected, and the neutral–neutral collisions are described by the hard sphere approximation. This approximation is justified since collisional cross-sections vary slowly at these energies, and since uncertainties introduced by the isotropic assumption are no larger than those of the various collision processes. Heat loss mechanisms, such as collisional excitation and subsequent radiation, are neglected.

As suggested in Nagy and Cravens (1981, 1988), the flux of suprathermal particles is divided into two components, an upward stream Φ^+ and a downward stream Φ^- (Schunk and Nagy, 2000). This approximation is justified given the uncertainties usually associated with the differential cross-sections. Considering that electric and magnetic fields can be neglected since neutral particles are modeled, and assuming steady state conditions, the two stream equation can be expressed by the following:

$$\langle \cos\theta \rangle \frac{\partial \Phi_s^+(E)}{\partial z} = -\sum_k n_k \sigma_{sk} \Phi_s^+(E)$$
$$+ P_s^{\text{casc}+}(E) + \frac{1}{2} P_s^{\text{chem}}(E),$$
$$-\langle \cos\theta \rangle \frac{\partial \Phi_s^-(E)}{\partial z} = -\sum_k n_k \sigma_{sk} \Phi_s^-(E)$$
$$+ P_s^{\text{casc}-}(E) + \frac{1}{2} P_s^{\text{chem}}(E), \tag{1}$$

where $\Phi_s^+(E)$ and $\Phi_s^-(E)$ are the upward and downward fluxes of suprathermal particle s carrying kinetic energy E, $\langle \cos\theta \rangle$ is the mean angle with respect to the vertical chosen to be 3/8 as suggested in Nagy and Banks (1970), σ_{sk} is the rigid sphere collisional cross-section of suprathermal particle s encountering target particle k of the cold background atmosphere, P_s^{chem} is the production term due to exothermic chemical reactions, assumed to be isotropic, and $P_s^{\text{casc}+}(E)$ and $P_s^{\text{casc}-}(E)$ are the cascading production terms from higher energy levels resulting in upward and downward particles, respectively.

As suggested by the term $\sum_k n_k \sigma_{sk} \Phi_s^{+,-}(E)$ in Eq. (1), a suprathermal particle with energy E is considered lost from its energy bin $E - \delta E/2$ to $E + \delta E/2$ whenever a collision occurs with the background gas. After the collision, the energy of particle s is degraded to a value lower than E, and its direction is modified such that in some cases an upward moving particle can be directed downward and vice-versa. This possible change of direction is taken into account by the variable $p_{sk}^b(E)$, the backscattering probability. The cascading production terms can therefore be expressed as follows:

$$P_s^{casc+}(E) = \sum_{E'} \sum_k n_k \sigma_{sk} \delta_{sk}(E', E)\left[(1 - p_{sk}^b)\Phi_s^+(E')\right.$$
$$\left. + p_{sk}^b \Phi_s^-(E')\right],$$
$$P_s^{casc-}(E) = \sum_{E'} \sum_k n_k \sigma_{sk} \delta_{sk}(E', E)\left[(1 - p_{sk}^b)\Phi_s^-(E')\right.$$
$$\left. + p_{sk}^b \Phi_s^+(E')\right], \tag{2}$$

where $\delta_{sk}(E', E)$ is equal to 0 by default and to 1 if the energy of suprathermal particle s, initially carrying energy E', is degraded to energy E after collision with background gas k. This quasi-linear approach is valid as long as the hot component is a small fraction of the net atmosphere in the exobase region, which is the case with chemistry-induced production.

In addition, if a particle of the thermal background gas is hit with sufficient energy, it can itself become suprathermal. Therefore, particles from the background atmosphere that gain sufficient energy after a collision with a hot particle must also be taken into account. This component can be modeled with Eqs. (1) and (2), but a production term must be added corresponding to the rate at which the initially thermal background particles become suprathermal:

$$P_k^{supra\pm}(E) = n_k \sum_{E'} \sum_s \sigma_{sk} \delta'_{sk}(E', E)\Phi_s^\pm(E'), \tag{3}$$

where $\delta'_{sk}(E', E)$ is equal to 0 by default and to 1 if the target thermal particle k is hit by suprathermal particle s, initially carrying energy E', and gains the suprathermal energy E as a result. Since the initial velocity of the target particle is zero relative to the bulk gas, the direction of its velocity after the energetic hard sphere collision is upward if the initial suprathermal particle was moving upward, and downward if it was moving downward.

Two cases were considered for the upper boundary condition. First, if the energy of the particle reaching the exobase in the upward direction is greater than the escape energy, the particle escapes from Titan's atmosphere. As a consequence, the downward flux in that energy bin at the exobase is zero. Second, if the energy of the particle at the exobase is lower than the escape energy, the particle is assumed to start a ballistic trajectory in the exosphere. This trajectory will lead it back to crossing the exobase a second time, but in the downward direction. Although particles crossing the exobase upward at one particular point in latitude and longitude have little chance to come back and cross the exobase again through the exact same point, it is assumed that the process is occurring uniformly: each particle crossing the exobase upward at one point is replaced by a second particle, moving downward, that follows in reverse the ballistic trajectory of the first particle. In other words, for all energy bins lower than the escape energy, the upper boundary is reflective and the rate of particles crossing the exobase upward is equal to the rate of particles coming back. The upper boundary condition can be expressed as follows:

$$E \geqslant E_{esc} \rightarrow \Phi_c^- = 0, \tag{4}$$
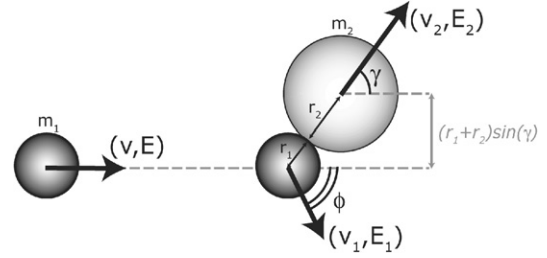$$E < E_{esc} \rightarrow \Phi_c^- = \Phi_c^+. \tag{5}$$

Fig. 1. Energy transfer and angular scattering during an elastic hard sphere collision.

where the subscript c refers to the altitude of the exobase, $E_{esc} = \frac{GM_{Titan}m}{R_{Titan}+z_c}$ is the escape energy, G is the gravity constant, M_{Titan} and R_{Titan} are the mass and the radius of Titan, and m is the mass of the suprathermal particle. At the lower boundary, it is assumed that collisions are sufficiently frequent for suprathermal particles to both be created, through exothermic chemistry, and thermalized, through elastic collisions with the background gas, essentially at the same location. In other words, transport becomes negligible and the flux of suprathermal particles is assumed to become isotropic at the lower boundary. In the two stream approximation, this condition is expressed as follows for all energy bins:

$$\Phi_0^- = \Phi_0^+. \tag{6}$$

The mechanisms of energy transfer and angular scattering occurring during elastic collisions were studied between two particles approximated as two hard spheres. The conservation of momentum and conservation of kinetic energy can be expressed with:

$$m_1 v = m_1 v_1 \cos\phi + m_2 v_2 \cos\gamma, \tag{7}$$
$$0 = -m_1 v_1 \sin\phi + m_2 v_2 \sin\gamma, \tag{8}$$
$$\frac{1}{2}m_1 v^2 = \frac{1}{2}m_1 v_1^2 + \frac{1}{2}m_2 v_2^2, \tag{9}$$

where a suprathermal particle with mass m_1, traveling with velocity v and kinetic energy E encountered a motionless background particle with mass m_2 (Fig. 1). After collision, if the distance between the centers of the two particles is $< r_1 + r_2$, the suprathermal particle m_1 travels with velocity v_1 in a direction deflected by angle ϕ, and target particle m_2 is put into motion with velocity v_2 in a direction parallel to the line between the two particles' centers at the moment of the impact, also characterized by angle γ. The post-collision energies E_1 and E_2 and the deflection angle ϕ can be expressed as:

$$E_1(\gamma) = \frac{m_1^2 + m_2^2 - 2m_1 m_2 \cos(2\gamma)}{(m_1 + m_2)^2} E, \tag{10}$$
$$E_2(\gamma) = \frac{4m_1 m_2 \cos^2(\gamma)}{(m_1 + m_2)^2} E, \tag{11}$$
$$\tan(\phi) = \frac{\sin(2\gamma)}{\frac{m_1}{m_2} - \cos(2\gamma)}. \tag{12}$$

The condition $\phi > \pi/2$ must be verified for particle m_1 to be backscattered after collision with particle m_2. Therefore, when $m_1 \geqslant m_2$, no backscattering is possible. However when

$m_1 < m_2$, the backscattering condition can be re-written using Eq. (12) as $\gamma < \frac{1}{2}\arccos(\frac{m_1}{m_2})$, and the backscattering probability p_{12}^b can be expressed as:

$$p_{12}^b = \int_0^{\frac{1}{2}\arccos(\frac{m_1}{m_2})} \sin(2\gamma)\,d\gamma = \frac{1}{2}\left(1 - \frac{m_1}{m_2}\right), \tag{13}$$

where $\sin(2\gamma)\,d\gamma$ is the probability for a collisional impact to occur between γ and $\gamma + d\gamma$. When $m_1 \geqslant m_2$, the average post-collision energies can be determined in a straightforward manner from Eqs. (10) and (11) for both the incoming and the target particles:

$$\langle E_1 \rangle = \frac{1}{\pi} \int_{-\pi/2}^{\pi/2} E_1(\gamma)\,d\gamma = \frac{m_1^2 + m_2^2}{(m_1 + m_2)^2} E, \tag{14}$$

$$\langle E_2 \rangle = \frac{1}{\pi} \int_{-\pi/2}^{\pi/2} E_2(\gamma)\,d\gamma = \frac{2m_1 m_2}{(m_1 + m_2)^2} E. \tag{15}$$

However, when $m_1 < m_2$, two cases must be considered. First, when m_1 is backscattered, the average post-collision energies can be expressed with:

$$\langle E_{b1} \rangle = \frac{1}{p_{12}^b} \int_0^{\frac{1}{2}\arccos(\frac{m_1}{m_2})} E_1(\gamma)\sin(2\gamma)\,d\gamma$$
$$= \frac{m_2(m_2 - m_1)}{(m_1 + m_2)^2} E, \tag{16}$$

$$\langle E_{b2} \rangle = \frac{1}{p_{12}^b} \int_0^{\frac{1}{2}\arccos(\frac{m_1}{m_2})} E_2(\gamma)\sin(2\gamma)\,d\gamma$$
$$= \frac{m_1(3m_2 + m_1)}{(m_1 + m_2)^2} E. \tag{17}$$

Second, when m_1 is not backscattered but forward-scattered, the average post-collision energies become:

$$\langle E_{f1} \rangle = \frac{1}{1 - p_{12}^b} \int_{\frac{1}{2}\arccos(\frac{m_1}{m_2})}^{\frac{\pi}{2}} E_1(\gamma)\sin(2\gamma)\,d\gamma = \frac{m_2}{m_1 + m_2} E, \tag{18}$$

$$\langle E_{f2} \rangle = \frac{1}{1 - p_{12}^b} \int_{\frac{1}{2}\arccos(\frac{m_1}{m_2})}^{\frac{\pi}{2}} E_2(\gamma)\sin(2\gamma)\,d\gamma = \frac{m_1}{m_1 + m_2} E. \tag{19}$$

In the present model, the fluxes of suprathermal particles are calculated per energy bin (in $cm^{-2}\,s^{-1}$). The width of the energy bins are chosen to be 10^{-2} eV between the thermal energy ($E_{th} \simeq 3.2 \times 10^{-2}$ eV) and 0.1 eV, 2×10^{-2} eV for the energy range 0.1–0.2 eV, 5×10^{-2} eV for 0.2–0.5 eV, 0.1 eV for 0.5–2 eV, 0.2 eV for 2–4 eV, and 0.5 eV between 4 eV and the maximum energy that particles could acquire from exothermic chemical mechanisms or background excitation. This maximum energy is as high as 9.5 eV for atomic and molecular hydrogen. The problem is solved in the form of a matrix equation for all the species simultaneously, using a column vector including all species and all energy bins. A first estimate of the downward stream is calculated assuming $\Phi^+ = 0$. This initial estimate accounts for the contribution of half of the chemical production. The upward stream is then calculated from bottom to top, accounting for the second half of the chemical production. Since most of the flux at low altitude comes from chemical production and not transport, only one update of the downward stream, this time shutting down the chemical production, is found necessary to compute the same lower boundary values as in the initial run.

3. Production terms for the hot particles modeled

In order to determine the production rates of hot N_2, CH_4, H, H_2, $^3CH_2$, CH_3, C_2H_4, C_2H_5, C_2H_6, $N(^4S)$, NH, and HCN, a one-dimensional composition model was built, describing interdependent ion and neutral densities for altitudes between 600 and 2000 km. 36 neutral species are modeled, undergoing vertical transport below the exobase. The temperature and eddy coefficient profiles are taken from De La Haye et al. (2007). The neutral density profiles are extended into the exosphere using a method based on the Liouville theorem (De La Haye et al., 2007; Schunk and Nagy, 2000). Dissociation and ionization schemes of the atmospheric neutrals by incoming solar photons and magnetospheric electrons are included, using an electron flux separately determined with the model of Gan et al. (1992). The neutral–neutral chemical mechanisms are based on Lebonnois et al. (2001) [updated in Lebonnois et al. (2003) and Lebonnois (2005)] and Wilson and Atreya (2004), and take into account revisions of the acetylene photodissociation scheme (Vuitton et al., 2006) and of the reaction rate of the main production mechanism for ethane, $CH_3 + CH_3 \xrightarrow{M} C_2H_6$, as suggested by Vuitton and Yelle (2005). At 600 km, the lower boundary, the mixing ratios were assumed to be fixed for all neutral species with a lifetime larger than one percent of a Titan rotational period—the lower boundary densities were adjusted to match adequately the INMS density measurements at higher altitudes (De La Haye et al., 2007) and mixing ratios were taken from Lebonnois et al. (2001) when no INMS data were available. For species with shorter lifetimes (for example $N(^4S)$ and NH), photochemical equilibrium was assumed as boundary condition.

The ion–neutral reactions involved in the present model are based on Keller et al. (1998). The ion species modeled (47) are assumed to be in photochemical equilibrium throughout the altitude range of the study. This assumption is justified since plasma transport effects only start being important above $\simeq 1450$ km, the altitude of the exobase (Cravens et al., 1998; Ma et al., 2004). In addition, Ma et al. (2004), who presented results from a 3D global MHD model of the interaction of Saturn's magnetospheric plasma with Titan's atmosphere, including 7 generic ionospheric species and some basic ion–neutral chemistry and ion–electron recombination, showed that the flow was primarily non-radial in the ionosphere due to the draping of the magnetic field lines around Titan.

The hot populations selected for investigation in the two stream model, were initially identified among the species resulting from the most energetic chemical reactions. These species include H, H_2, $^3CH_2$, CH_3, C_2H_4, C_2H_5, C_2H_6, $N(^4S)$, NH, and HCN. The rigid-sphere collisional diameters of these species were determined with the formula of Hirschfelder et al. (1954), that gives a first-order approximation of the viscosity of a pure gas:

$$\eta \times 10^7 = 266.93 \frac{\sqrt{MT}}{(2R)^2}, \tag{20}$$

where η is the viscosity of the gas ($g\,cm^{-1}\,s^{-1}$), M is the molecular mass (amu), T is the gas temperature (K), and R is the rigid-sphere molecular radius (Å). When viscosity data were accessible, the rigid-sphere collisional radii were determined with Eq. (20) and listed in Table 1. Values corresponding to 150 K were chosen when they were available. For atomic species H, C, and N, the atomic radii were taken from ACS (ACS, 2005. Chemistry.org, the website of the American Chemical Society. On the Web. http://center.acs.org/periodic/tools/PT.html). No viscosity data were found for the radical species listed above, and approximations had to be made: the rigid sphere radius of CH_4 was attributed to CH_3 and $^3CH_2$, and the sum of the radii of atomic nitrogen and hydrogen was used for NH.

In order to estimate the influence of the uncertainty on rigid sphere radii, a sensitivity study was conducted on the value chosen for the main constituent: molecular nitrogen. The study was performed by modeling hot hydrogen, nitrogen and methane molecules traveling through a background mixture of nitrogen and methane. Three nitrogen molecular radii were chosen as successive parameters to the two stream model: 2.07 Å, the value calculated with Eq. (20), 1.88 Å, the value corresponding to a diameter of 3.75 Å as sometimes listed in the literature (Hirschfelder et al., 1954), and 1.97 Å, an intermediate value. The variation obtained using three different rigid sphere radii of molecular nitrogen was found to be lower than 5% for the logarithms of the densities. It was therefore concluded that the influence of the molecular nitrogen radii is negligible compared to other uncertainties such as more accurate angular differential cross-sections (Shematovich and Johnson, 2006) or the reaction rates, in particular, the electron recombination rates. In the end, the values listed in Table 1 are assumed sufficient to obtain meaningful estimates of suprathermal fluxes and density profiles.

For each selected hot particle, the production term P_{chem} is determined using all chemical reactions involved in the coupled ion and neutral model. The enthalpy of formation used to determine the exothermicities are taken from Chase (1998), Burcat (2001), Lias et al. (1988), and McEwan and Phillips (1975). The exothermic energy of each reaction is assumed to be shared between the produced particles in the form of kinetic energy only, divided inversely with their mass. Therefore, the present calculations represent an upper-bound estimate of the corona induced by exothermic chemistry. Since the number of mechanisms that can be presented is constrained, the focus is placed on detailing the reactions producing large amounts of one specific hot

Table 1
Hard sphere radius for major species present in Titan's upper atmosphere

Species	Viscosity[b] ($10^7\,g\,cm^{-1}\,s^{-1}$)		Hard sphere radius (cm)
H	–		7.8×10^{-9}[a]
H_2	554.85	(150 K)	1.44×10^{-8}
C	–		7.7×10^{-9}[a]
CH_4	592.89	(150 K)	2.35×10^{-8}
C_2H_4	571.37	(170 K)	2.84×10^{-8}
C_2H_6	470.92	(150 K)	3.08×10^{-8}
$N(^4S)$	–		0.74×10^{-8}[a]
N_2	1011.8	(150 K)	2.07×10^{-8}
HCN	257.57	(300 K)	4.83×10^{-8}

[a] ACS, 2005. Chemistry.org, the website of the American Chemical Society. On the Web. http://center.acs.org/periodic/tools/PT.html.
[b] Rowley et al. (2003).

species, and the reactions producing hot particles with large kinetic energy. In particular, the cases of hot N_2, CH_4, H_2, H, C_2H_6, and HCN are examined below.
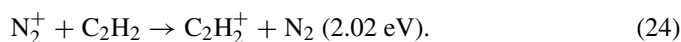
The production rate profiles of the main mechanisms producing hot N_2 are presented in Fig. 2 for the T_A conditions, at noon local time, latitude 38° North, zenith angle 61.7°. In this figure, as well as in the following production rate plots, the neutral bimolecular mechanisms are represented with solid lines, the ion–neutral production rates with large-dotted lines, the electron recombination rates with a variety of dashed lines, and the neutral termolecular mechanisms with triangles. The processes most efficient at producing a large amount of hot N_2 below 1250 km, involve quenching by nitrogen of the excited species $^1CH_2$ and $N(^2D)$:

$$^1CH_2 + N_2 \rightarrow \,^3CH_2 + N_2 \,(0.11\,eV), \tag{21}$$

$$N(^2D) + N_2 \rightarrow N(^4S) + N_2 \,(0.79\,eV), \tag{22}$$
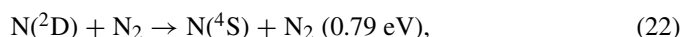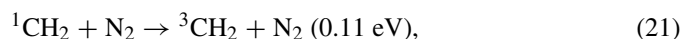
where the energies in parenthesis are the kinetic energy attributed to the nitrogen molecule as a result of these reactions, and knowing that process (21) disappears on the night side. At altitudes above 1250 km, the following ion–neutral process becomes dominant:

$$N_2H^+ + CH_4 \rightarrow CH_5^+ + N_2 \,(0.23\,eV). \tag{23}$$
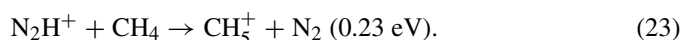
The hottest nitrogen molecules produced by chemistry reach a kinetic energy of 2.02 eV, and result from the ion–neutral process:

$$N_2^+ + C_2H_2 \rightarrow C_2H_2^+ + N_2 \,(2.02\,eV). \tag{24}$$

The production rate of this mechanism is about two to three orders of magnitude lower than the previous ones. Higher energy (5–5.5 eV) may be gained by the cold nitrogen molecules of the background atmosphere after they are hit by other suprathermal molecules traveling through Titan's upper atmosphere.

Among the exothermic chemical mechanisms producing hot CH_4 molecules (Fig. 3), the higher production rates are found to be attributed to the four following mechanisms:

$$CH_5^+ + e^- \rightarrow CH + CH_4 \,(0.46\,eV), \tag{25}$$

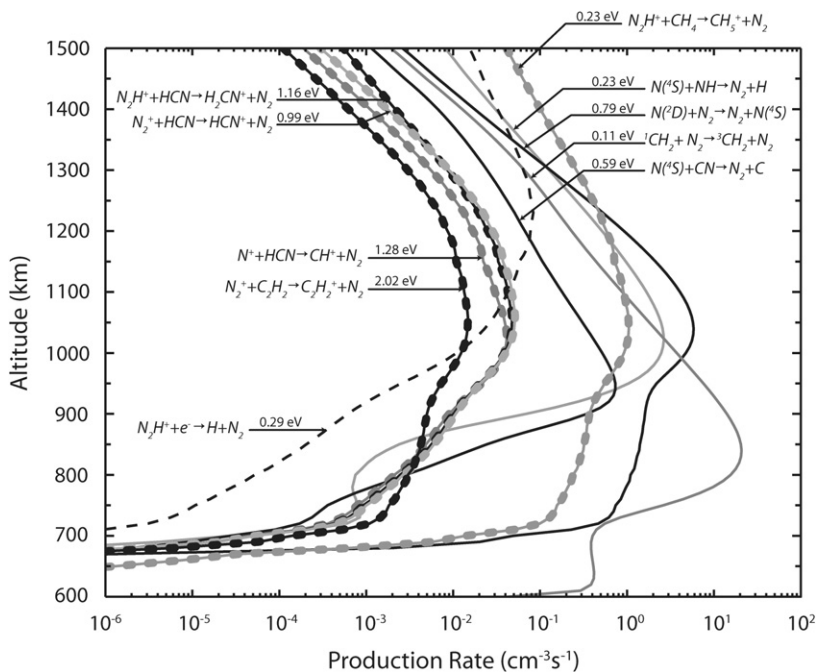$$C_2H_5^+ + C_2H_4 \rightarrow C_3H_5^+ + CH_4 \,(0.63\,eV), \tag{26}$$
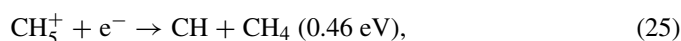
Fig. 2. Production rate profiles for hot nitrogen molecules, resulting from a selection of the most important exothermic chemical reactions—the kinetic energy given to N_2 is indicated for each reaction.
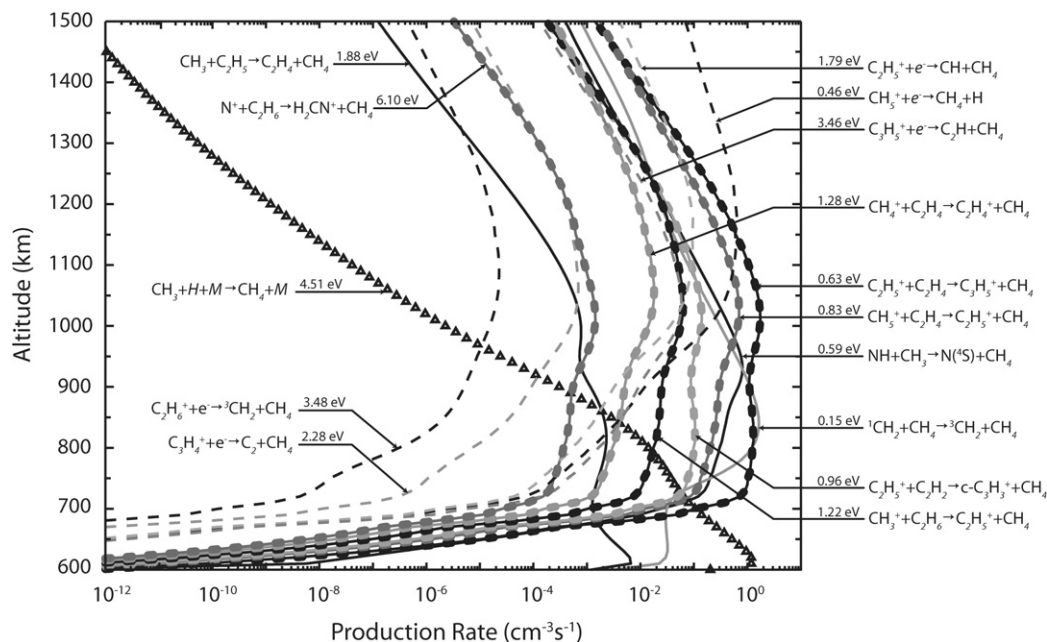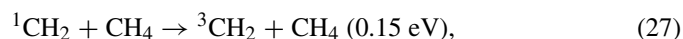

Fig. 3. Production rate profiles for hot methane molecules, resulting from a selection of the most important exothermic chemical reactions—the kinetic energy given to CH_4 is indicated for each reaction.

$$^1CH_2 + CH_4 \rightarrow {}^3CH_2 + CH_4 \ (0.15 \ eV), \tag{27}$$

$$CH_3 + H \xrightarrow{M} CH_4 \ (4.51 \ eV), \tag{28}$$

which dominate above 1150 km for process (25), between 700 and 1150 km for process (26), except for the altitude range 800 to 900 km where process (27) prevails, and between 600 and 700 km for process (28). The hottest chemistry-produced methane molecules are found to reach 6.10 eV and to be produced by the ion–neutral reaction:

$$N^+ + C_2H_6 \rightarrow H_2CN^+ + CH_4 \ (6.10 \ eV). \tag{29}$$

The production rate of this mechanism, however is about five orders of magnitude lower than the peak production rates of mechanisms (25) to (28).

The production rates of hot molecular hydrogen by exothermic chemical reactions (Fig. 4) are dominated by two processes, the first involving neutral chemistry and the second dealing with ion–neutral chemistry:
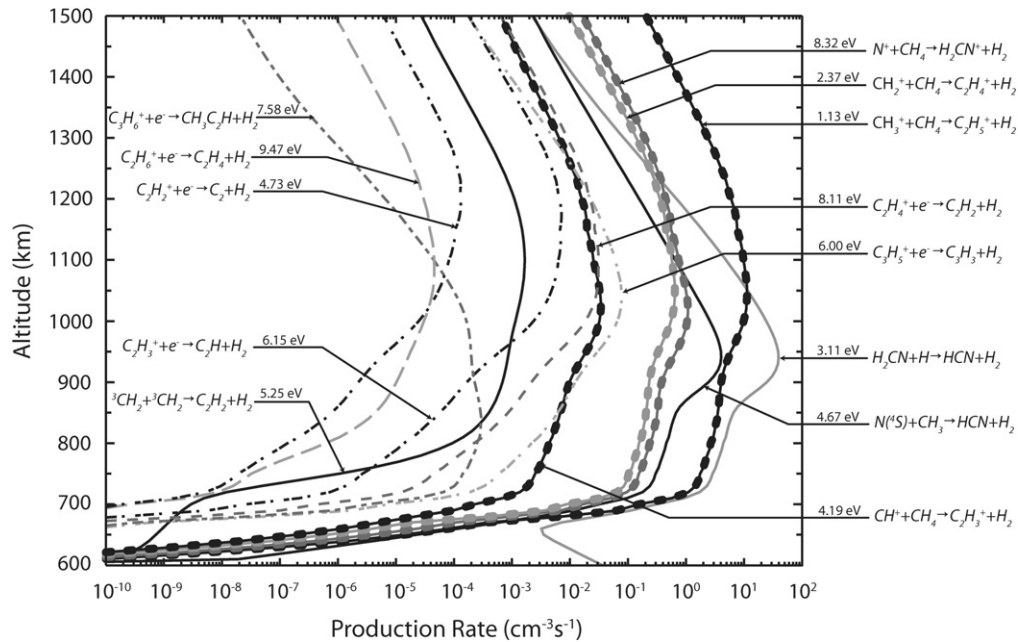
Fig. 4. Production rate profiles for hot hydrogen molecules, resulting from a selection of the most important exothermic chemical reactions—the kinetic energy given to H_2 is indicated for each reaction.
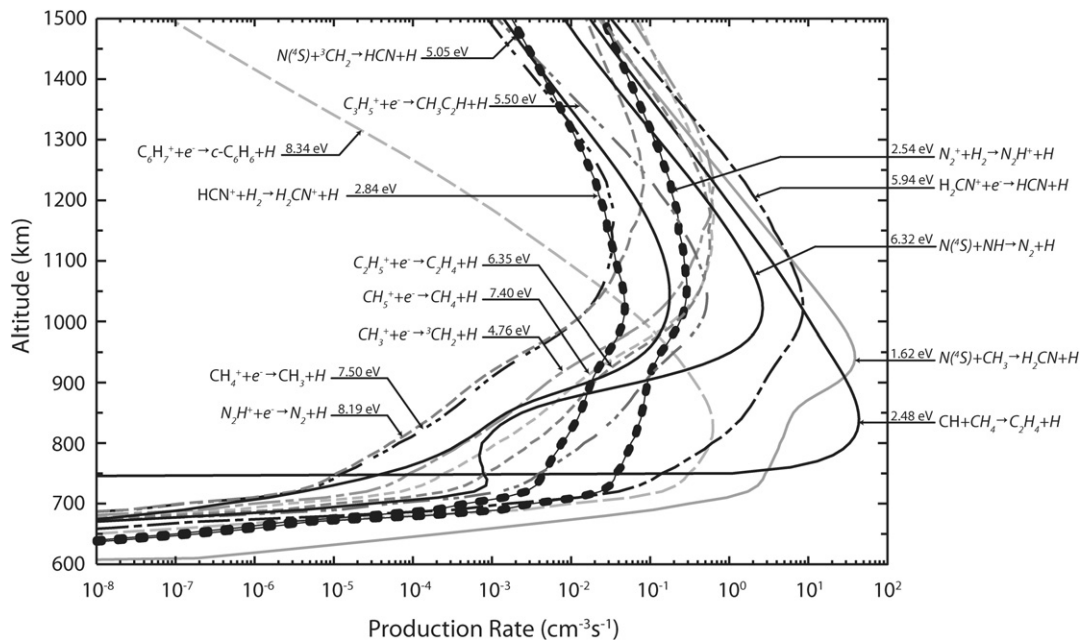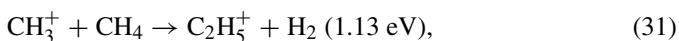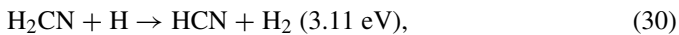

Fig. 5. Production rate profiles for hot hydrogen atoms, resulting from a selection of the most important exothermic chemical reactions—the kinetic energy given to H is indicated for each reaction.

$$H_2CN + H \rightarrow HCN + H_2 \ (3.11 \ eV), \tag{30}$$

$$CH_3^+ + CH_4 \rightarrow C_2H_5^+ + H_2 \ (1.13 \ eV), \tag{31}$$

which alternatively dominate below and above 1050 km, respectively. The reaction producing the hottest hydrogen molecules is found to be:

$$C_2H_6^+ + e^- \rightarrow C_2H_4 + H_2 \ (9.47 \ eV), \tag{32}$$
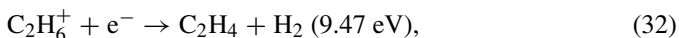
but here again with a production rate about five orders of magnitude lower than the peak production rates of processes (30) and

(31). The critical exothermic reaction for producing hot hydrogen molecules is:

$$N^+ + CH_4 \rightarrow H_2CN^+ + H_2 \ (8.32 \ eV), \tag{33}$$
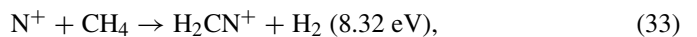
which produces hot hydrogen molecules with an energy only 1.15 eV lower than process (32), but with a production rate four orders of magnitude larger. Since molecular hydrogen is the third most abundant species in Titan's upper atmosphere after nitrogen and methane, it was also considered as a background species in the model. The collisions of the hot modeled
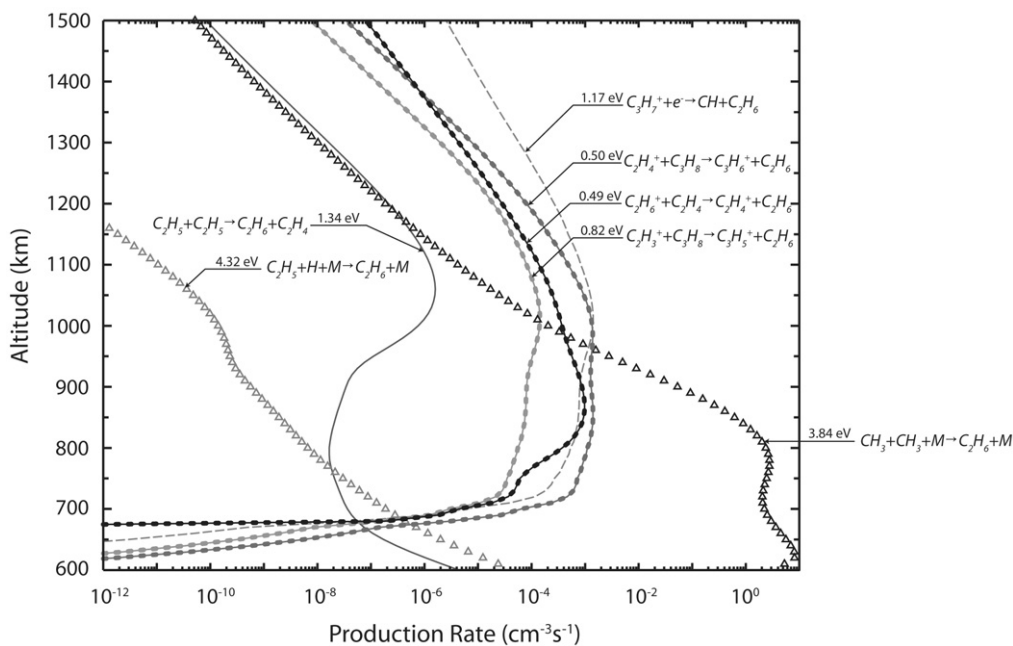
Fig. 6. Production rate profiles for hot ethane molecules, resulting from a selection of the most important exothermic chemical reactions—the kinetic energy given to C_2H_6 is indicated for each reaction.
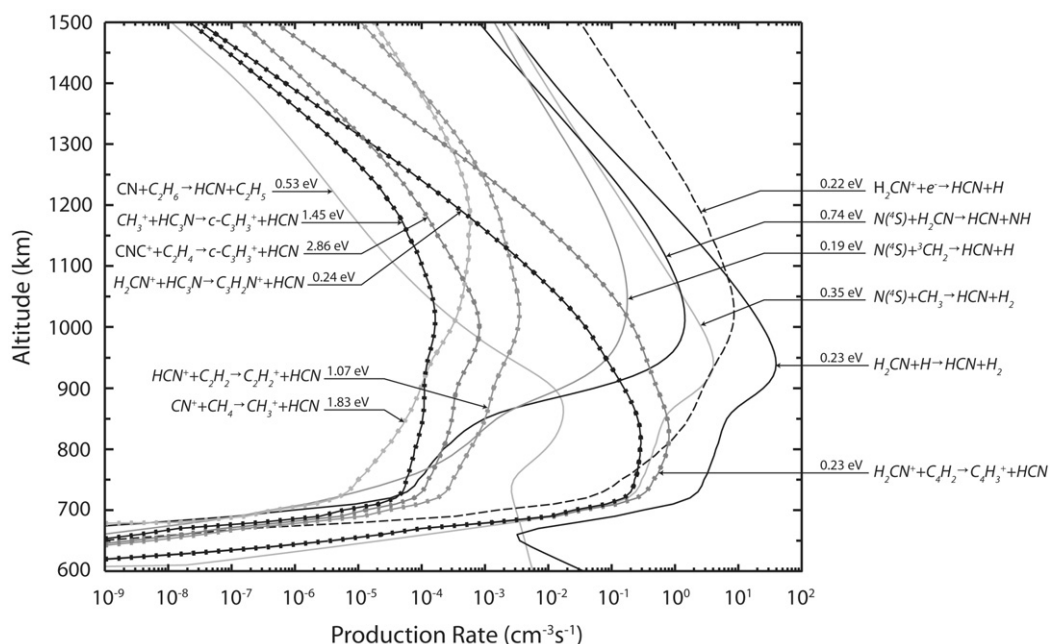

Fig. 7. Production rate profiles for hot hydrogen cyanide molecules, resulting from a selection of the most important exothermic chemical reactions—the kinetic energy given to HCN is indicated for each reaction.
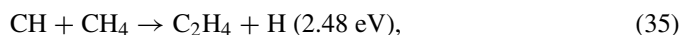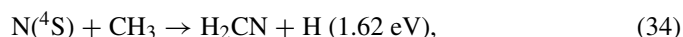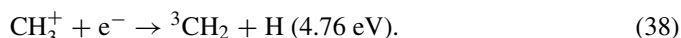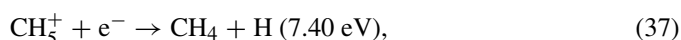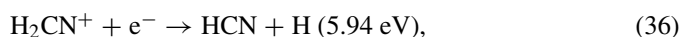
particles with these cold H_2 molecules are found to represent a production process for hot H_2 comparable to chemistry over the altitude range of the study.

Hot hydrogen atoms are produced by a large number of chemical reactions, dominated by neutral chemistry mechanisms at low altitudes and electron recombination mechanisms at high altitudes (Fig. 5). The reactions with the most important production rates below $\simeq 1100$ km are:

$$N(^4S) + CH_3 \rightarrow H_2CN + H \ (1.62 \text{ eV}), \tag{34}$$

$$CH + CH_4 \rightarrow C_2H_4 + H \ (2.48 \text{ eV}), \tag{35}$$

and above $\simeq 1100$ km:

$$H_2CN^+ + e^- \rightarrow HCN + H \ (5.94 \text{ eV}), \tag{36}$$

$$CH_5^+ + e^- \rightarrow CH_4 + H \ (7.40 \text{ eV}), \tag{37}$$

$$CH_3^+ + e^- \rightarrow {}^3CH_2 + H \ (4.76 \text{ eV}). \tag{38}$$

The other mechanism of importance is the reaction producing the hottest hydrogen atoms (8.34 eV), whose production rate
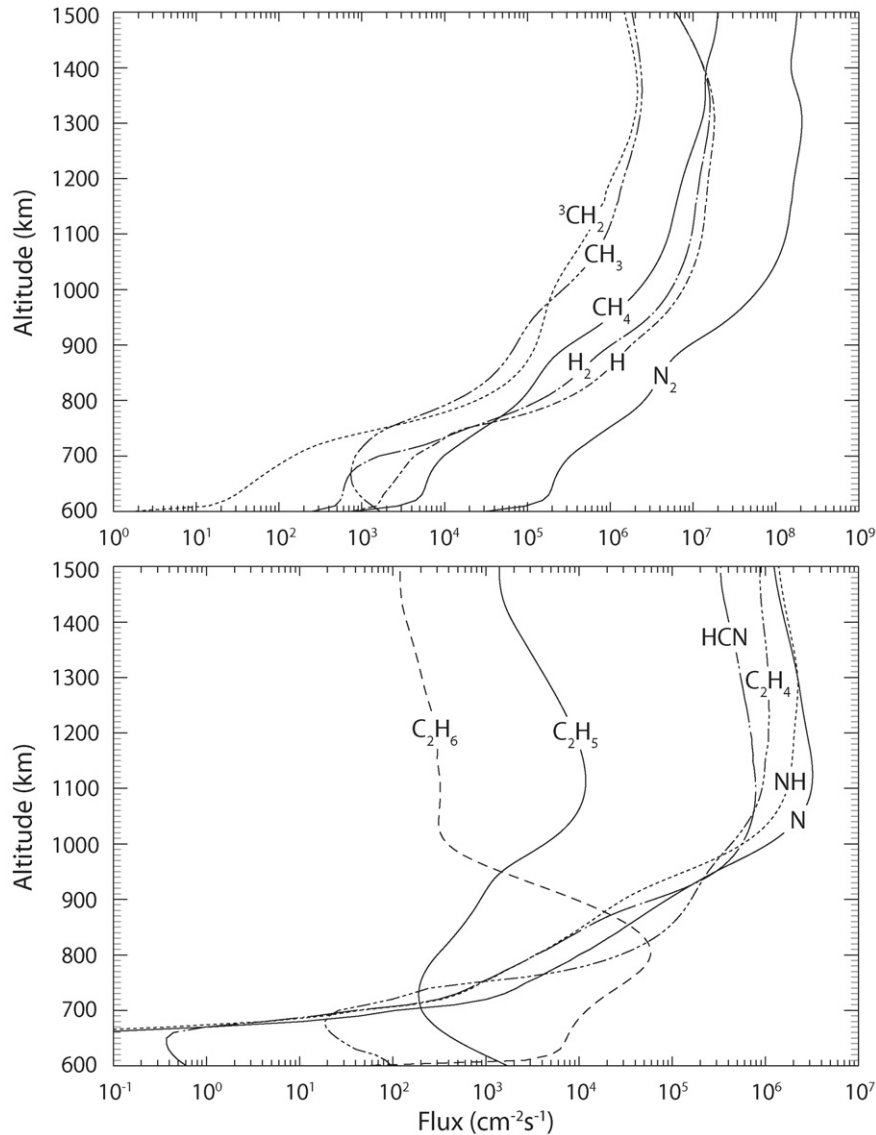
Fig. 8. Sum of the upward and downward suprathermal fluxes for all energy bins resulting from the two stream model, describing the fate of 12 hot species produced by exothermic chemistry traveling through Titan's upper atmosphere (back ground mixture of N_2, CH_4, and H_2). Hot species N_2, CH_4, H, H_2, $^3CH_2$, and CH_3 are presented in the upper panel, and hot species C_2H_4, C_2H_5, C_2H_6, N, NH, and HCN in the lower panel.

competes with the peak production rates of the afore-mentioned reactions within two orders of magnitude at 800 km:

$$C_6H_7^+ + e^- \rightarrow c\text{-}C_6H_6 + H \ (8.34 \text{ eV}). \tag{39}$$
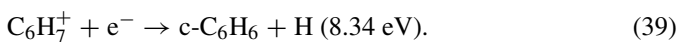
Hot C_2H_6 molecules are produced with a high energy and a large production rate by the termolecular mechanism (Fig. 6):

$$CH_3 + CH_3 \xrightarrow{M} C_2H_6 \ (3.84 \text{ eV}). \tag{40}$$
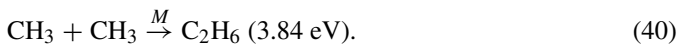
However, the mechanism producing the hottest C_2H_6 molecules is another termolecular process involving C_2H_5, but its production rate is about five orders of magnitude lower than reaction (40):

$$C_2H_5 + H \xrightarrow{M} C_2H_6 \ (4.32 \text{ eV}). \tag{41}$$
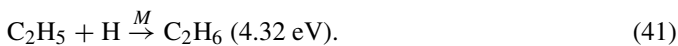
Mechanism (40) dominates the production rates for all hot ethane molecules up to 950 km. Above this altitude, the process taking over involves electron recombination:

$$C_3H_7^+ + e^- \rightarrow CH + C_2H_6 \ (1.17 \text{ eV}). \tag{42}$$
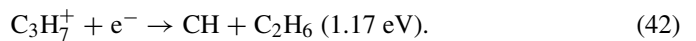
Finally, the production rate profiles of the exothermic reactions leading to the formation of suprathermal HCN molecules are plotted in Fig. 7. The two mechanisms dominating the production rates of hot HCN are found to be:

$$H_2CN^+ + e^- \rightarrow H + HCN \ (0.22 \text{ eV}), \tag{43}$$

$$H_2CN + H \rightarrow H_2 + HCN \ (0.23 \text{ eV}), \tag{44}$$
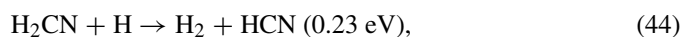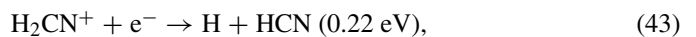
which dominate above and below $\simeq 1075$ km, respectively. The hottest hydrogen cyanide molecules reach the energy of 2.86 eV and are produced by the following exothermic ion–neutral mechanism:

$$CNC^+ + C_2H_4 \rightarrow c\text{-}C_3H_3^+ + HCN \ (2.86 \text{ eV}). \tag{45}$$

Fig. 9. Suprathermal density profiles resulting from the two stream model, that describes the fate of 12 hot species produced by 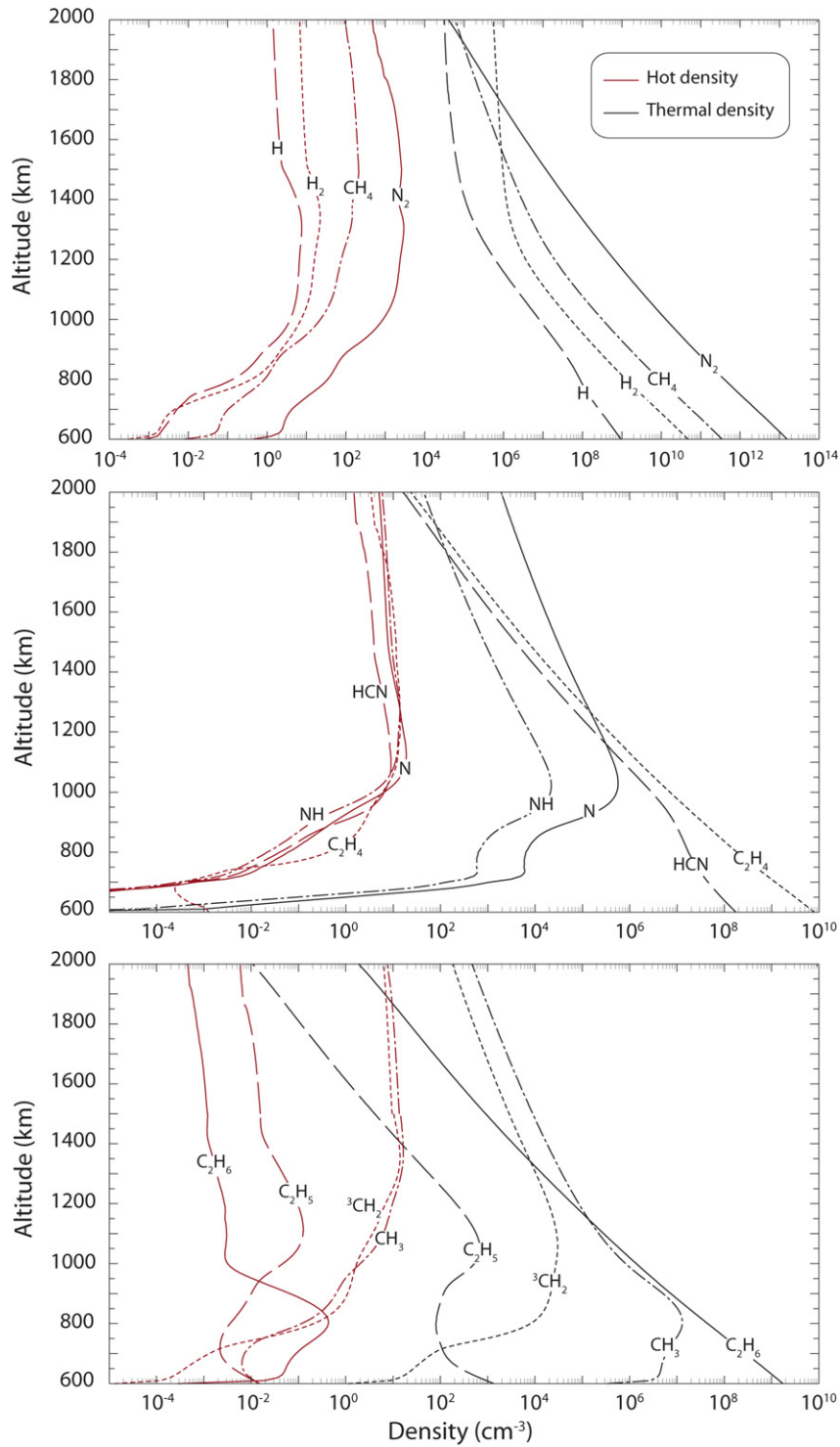exothermic chemistry traveling through Titan's upper atmosphere (back ground mixture of N_2, CH_4, and H_2). The density profiles of the hot particles are plotted in red and are compared to the corresponding thermal profiles, plotted in black. Species N_2, CH_4, H_2, and H are represented in the upper panel, N, NH, HCN, and C_2H_4 in the middle panel, and $^3CH_2$, CH_3, C_2H_5, and C_2H_6 in the lower panel.

4. Results and discussion

The hot flux, density and energy distribution presented in this section were calculated using the T_A solar and latitudinal conditions (latitude 38° North and zenith angle 61.7° at noon local time), and taking into account both photo- and magnetospheric electrons as energy inputs for the chemical ion and neutral coupled model.

The total suprathermal fluxes resulting from the two-stream calculation, i.e., the sum of the upward and downward fluxes

Table 2
Density of the hot populations produced by exothermic chemical reactions at the exobase, and comparison with results obtained by fitting the INMS exospheric data

Species		Hot density (cm^{-3})	Escape flux (s^{-1})	Species	Hot density (cm^{-3})	Escape flux (s^{-1})
N$_2$	This model	2.4×10^3	2.1×10^{24}	H$_2$	1.5×10^1	2.8×10^{25}
	De La Haye et al. (2007)	$4.4 \pm 5.1 \times 10^5$	$8.5 \pm 7.0 \times 10^{25}$	H	4.0	1.5×10^{25}
				^{3}CH$_2$	1.2×10^1	1.9×10^{24}
				CH$_3$	1.6×10^1	1.1×10^{24}
CH$_4$	This model	1.9×10^2	2.5×10^{24}	C$_2$H$_4$	1.2×10^1	5.1×10^{23}
	De La Haye et al. (2007)	$1.1 \pm 0.9 \times 10^5$	$5.9 \pm 5.3 \times 10^{25}$	C$_2$H$_5$	1.6×10^{-2}	2.8×10^{23}
				C$_2$H$_6$	1.2×10^{-3}	4.2×10^{22}
				N	8.4	2.2×10^{24}
				NH	9.9	1.1×10^{24}
				HCN	4.1	7.5×10^{23}

Notes. The values in De La Haye et al. (2007) are the averaged suprathermal density and escape fluxes derived from fitting the exospheric T_A, T_B, and T_5 INMS data. The globally averaged escape fluxes are estimated here using an exobase area of $\simeq 2.1 \times 10^{18}$ cm^2, where the altitude of the exobase is assumed to be 1450 km.

with all energy bins added, are plotted as a function of altitude for hot species N$_2$, CH$_4$, H, H$_2$, ^{3}CH$_2$, CH$_3$, C$_2$H$_4$, C$_2$H$_5$, C$_2$H$_6$, N(^{4}S), NH, and HCN in Fig. 8. The large N$_2$ and CH$_4$ hot fluxes are due, in particular, to the high density of their thermal component, which becomes suprathermal through excitation of the background gas. The fluxes of suprathermal H and H$_2$, are found to be larger than the flux of suprathermal CH$_4$, but weaker than the flux of suprathermal N$_2$. They are critical because they carry most of the kinetic energy due to their low mass. For all suprathermal species except C$_2$H$_6$ and C$_2$H$_5$, a similar trend increasing with altitude and plateauing between 1000 and 1200 km, is observed. The fluxes of hot C$_2$H$_6$ and C$_2$H$_5$ are found to be significantly smaller than the other species at high altitudes, their production being mainly due to termolecular reactions below 900 km.

The density profiles of the hot components were calculated below the exobase using:

$$n_{hot} = \sum_E \left(\Phi^+(E) + \Phi^-(E) \right) \sqrt{\frac{m}{2E}}. \tag{46}$$

Knowing the energy distribution at the exobase, the hot density profiles were then extended between 1450 and 2000 km using a method based on the Liouville theorem described in De La Haye et al. (2007) and Schunk and Nagy (2000). The hot density profiles are plotted and compared with the particles' thermal components in Fig. 9. The hot components are found to be several orders of magnitude smaller than the thermal profiles throughout the altitude range of the study. At 2000 km, the fraction of the hot versus thermal density for each species is: 1.3% for N$_2$, 0.15% for CH$_4$, 1.3×10^{-5} for H$_2$, 5.0×10^{-5} for H, 2.3×10^{-4} for C$_2$H$_6$, 2.5×10^{-3} for NH, 1.5% for CH$_3$, 3.2% for ^{3}CH$_2$, 9.0% for HCN, 13% for N, 14% for C$_2$H$_4$, and 60% for C$_2$H$_5$. Therefore, except for neutral species C$_2$H$_5$, the production of suprathermal particles by exothermic chemistry does not alter significantly the neutral density profiles of Titan's upper atmosphere and lower exosphere.

The suprathermal density and global escape fluxes obtained at the exobase are reported in Table 2. The global loss of nitrogen atoms in all forms due to exothermic chemistry is found to be $\simeq 8.3 \times 10^{24}$ N s^{-1}, mainly due to the escape of N$_2$, N, and NH. This value is $\simeq 3$ times smaller than the nitro-

gen escape rate (2.5×10^{25} N s^{-1}) reported in Cravens et al. (1997). The global loss of carbon atoms in all forms is found to be $\simeq 7.2 \times 10^{24}$ C s^{-1}, with the largest contribution coming from escaping CH$_4$ molecules, followed by ^{3}CH$_2$, CH$_3$, and C$_2$H$_4$. This value is two to six times smaller than the range 1.7–4×10^{25} s^{-1} estimated in Cravens et al. (1997). In addition to electron recombination and ion–neutral reactions, which were taken into account as hot production mechanisms in Cravens et al. (1997), the present model takes into account the heating contribution of exothermic neutral–neutral reactions. The lower escape rates inferred in the present work must therefore be explained by factors other than the choice of chemical production mechanisms. These factors probably involve the use of a two-stream calculation compared to the integration of the production rates performed in Cravens et al. (1997), and the use of different solar incoming fluxes, i.e., solar maximum (Voyager flyby in November 1981) in Cravens et al. (1997), compared to solar minimum (Cassini T_A flyby in October 2004) in the present work. Overall, the global losses of nitrogen and carbon atoms due to exothermic chemistry are found to be consistent with those estimated by Cravens et al. (1997).

The contribution of exothermic chemistry to Titan's corona, initiated by incoming photons and magnetospheric electrons, is found to be significant with respect to that of sputtering. The escape rate of nitrogen atoms in all forms due to exothermic chemistry is found to represent about a quarter of the maximum escape 3.6×10^{25} N s^{-1} inferred by Shematovich et al. (2003) when taking into account sputtering and photodissociation, or the sputtering-induced escape 3.7×10^{25} N s^{-1} estimated by Michael et al. (2005) using the N$^+$ and N$_2^+$ fluxes of Brecht et al. (2000).

As shown in Table 2, the N$_2$ and CH$_4$ suprathermal densities induced by exothermic chemistry are about two and three orders of magnitude smaller, respectively, than the average values estimated in De La Haye et al. (2007) from the fit of the INMS T_A, T_B, and T_5 data ($4.4 \pm 5.1 \times 10^5$ cm^{-3} for hot N$_2$ and $1.1 \pm 0.9 \times 10^5$ cm^{-3} for hot CH$_4$). The suprathermal populations produced by exothermic chemistry are therefore insufficient to justify the INMS observations, and in particular the change of slope observed above 1600 km in the N$_2$ and CH$_4$ density profiles. The modeled N$_2$ and CH$_4$ escape
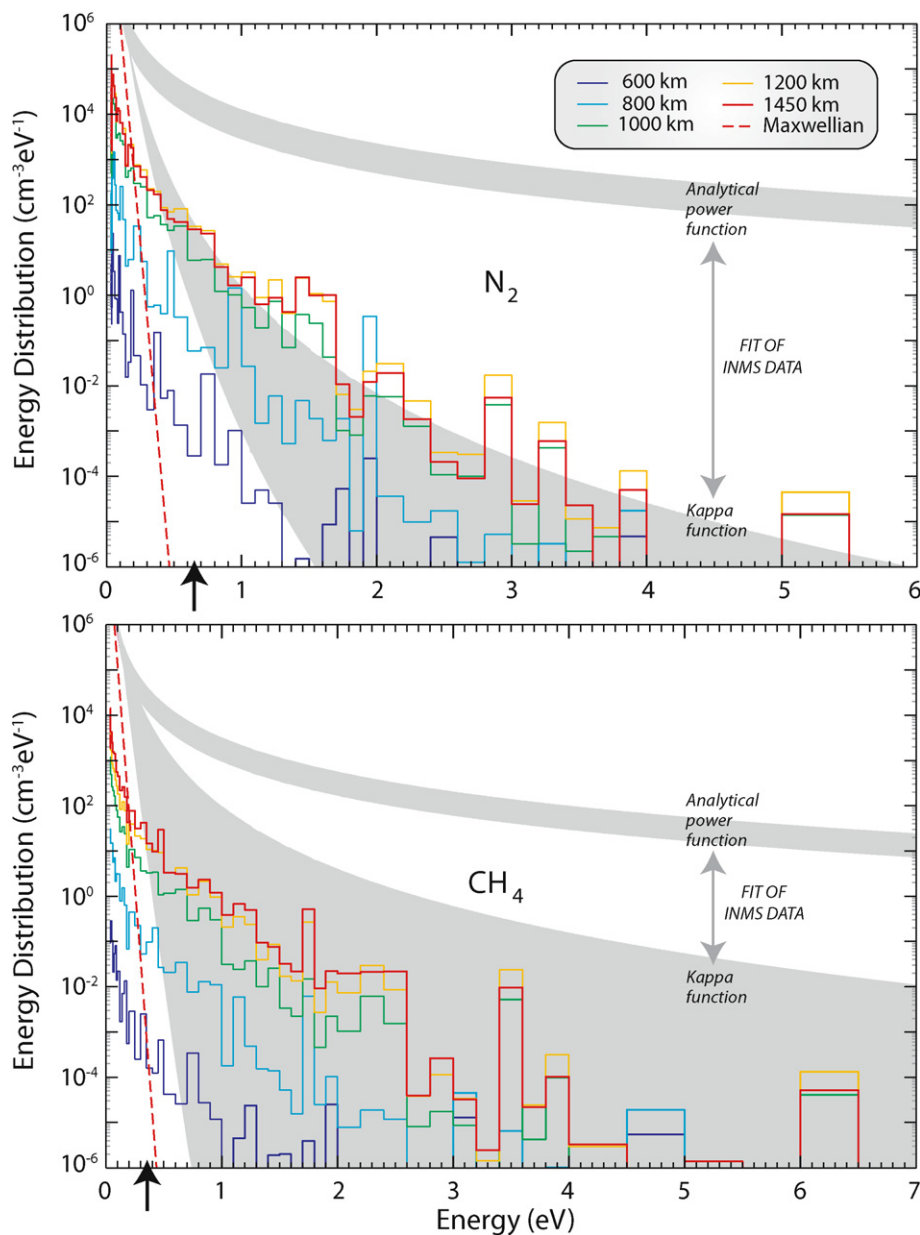
Fig. 10. Energy distribution of the hot N_2 and CH_4 particles produced by exothermic chemistry in Titan's upper atmosphere and modeled using the two stream model. Profiles are shown at altitudes 600, 800, 1000, 1200, and 1450 km (the altitude corresponding to the exobase). On each graph, the Maxwellian distribution is plotted for comparison with a red dashed line, and the escape energy at the exobase is indicated with an arrow. The gray areas correspond to the range of INMS data fits obtained in De La Haye et al. (2007) using two different energy distribution functions at the exobase, an analytical function, and a kappa function.

fluxes are found to be about 40 and 25 times smaller, respectively, than the average values estimated in De La Haye et al. (2007) by multiplying the energy deposition rates inferred from the INMS data, by the ratio of the escape rate in Michael et al. (2005) to the energy deposition rate in Michael and Johnson (2005). The N_2 escape flux value is however $\simeq 15$ times greater than the averaged lower bound estimated in De La Haye et al. (2007) by using a kappa function as exobase energy distribution (i.e. $\simeq 1.5 \times 10^{23}$ $N_2\,s^{-1}$ assuming an exobase area of 2.1×10^{18} cm^2).

The energy distributions of chemistry-induced hot N_2 and CH_4 are plotted in Fig. 10 for altitude levels 600, 800, 1000, 1200, and 1450 km (the altitude of the exobase). These profiles

are compared to the data fit results of De La Haye et al. (2007), the gray areas representing the range of values obtained from the T_A ingress and egress, T_B egress, and T_5 egress distributions at the exobase, using either an analytical model or a kappa function. The escape energies are represented on the x-axes with a vertical arrow, and the Maxwellian distributions are plotted, allowing to gauge the extent of the suprathermal tails. At high energy ($E > 1$ eV), the energy distribution induced by exothermic chemistry is found to lie within the range predicted by the study of INMS data. The main difference between model and data-fit appears at lower energy, $E < 0.3$–0.4 eV. Both modeled N_2 and CH_4 distributions depart from the Maxwellian at energy > 0.2 eV, where the number of particles is $\simeq 10^3$ cm^{-3}
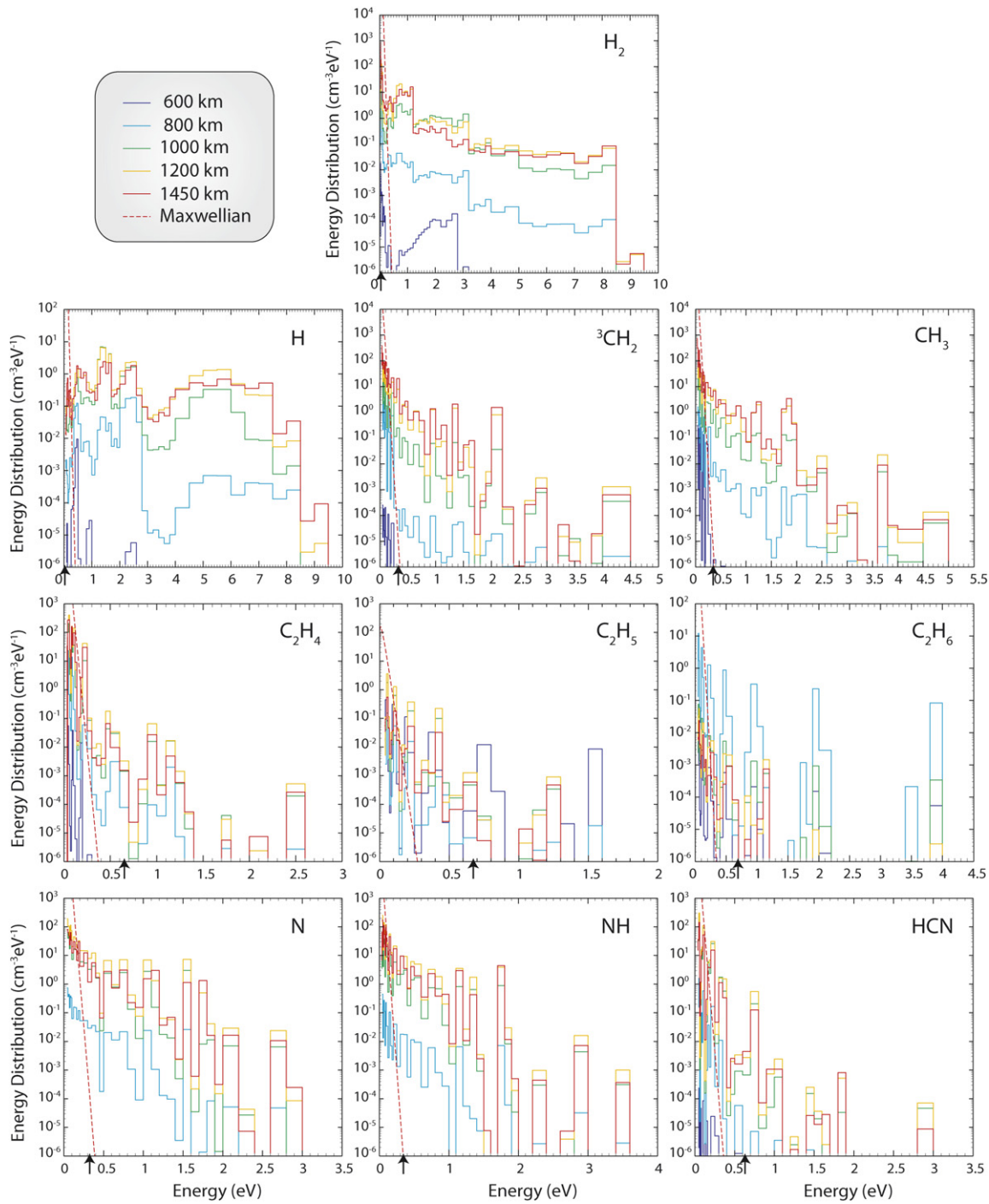
Fig. 11. Energy distribution of the hot H_2, H, $^3CH_2$, CH_3, C_2H_4, C_2H_6, $N(^4S)$, NH, and HCN particles produced by exothermic chemistry in Titan's upper atmosphere and modeled using the two stream model. Profiles are shown at altitudes 600, 800, 1000, 1200, and 1450 km (the altitude corresponding to the exobase). On each graph, the Maxwellian distribution is plotted for comparison with a red dashed line, and the escape energy at the exobase is indicated with an arrow.

for N_2 and $\simeq 10^2$ cm^{-3} for CH_4. By comparison, the distributions inferred from the fit of INMS data depart from the Maxwellian at lower energy, corresponding to a number of particles of $\simeq 10^6$ cm^{-3}, three orders of magnitude larger. So the source of suprathermal neutrals induced by exothermic chemistry appears insufficient to justify the high number of low energy suprathermal particles detected in the INMS observations.

The energy distributions of hot H, H_2, $^3CH_2$, CH_3, C_2H_4, C_2H_5, C_2H_6, $N(^4S)$, NH, and HCN, resulting from exothermic chemistry, are plotted in Fig. 11. Comparisons with the Maxwellian profiles show the presence of significant suprathermal populations throughout Titan's upper atmosphere. The escape energy values (indicated with a vertical arrow on each x-axis), suggest that Titan's corona is populated by a variety of neutrals resulting from the complex neutral and ion chemistry

that takes place in the upper atmosphere. The energies of the hot N and N_2 are lower when produced by exothermic chemistry as compared to sputtering: in the present study, neutrals N and N_2 are found to reach maximum energies of 3 and 5.5 eV, respectively, whereas Shematovich et al. (2003) calculated average energies of 6.43 and 6.90 eV for hot N, and 2.21 and 6.9 eV for hot N_2, due to sputtering by magnetospheric ions N^+ and $C_2H_5^+$.

5. Conclusions

In the present work, the contribution of complex neutral–neutral and ion–neutral chemistry to Titan's corona was studied. Detailed production rate profiles were calculated using a coupled ion–neutral model, and a two stream model was constructed to model the fate of 12 suprathermal particles traveling through a background mixture of cold N_2, CH_4, and H_2. We found that Titan's corona is populated by a variety of hot neutrals induced by exothermic chemistry, with suprathermal density and escape fluxes that are significant with respect to sputtering. The nitrogen loss represents about a quarter of that produced by estimates of pick-up ion sputtering (Michael et al., 2005). The global loss of nitrogen atoms in all forms is $\simeq 8.3 \times 10^{24}$ $N\,s^{-1}$ and the global loss of carbon atoms $\simeq 7.2 \times 10^{24}$ $C\,s^{-1}$. These values are in average 3 and 4 times smaller than those estimated in Cravens et al. (1997), mainly due to differences in methods (two-stream calculation vs production rate integration) and solar inputs.

The consideration of the energy released by exothermic chemical reactions alone is shown to be insufficient for producing the significant N_2 and CH_4 suprathermal populations observed by INMS in the exosphere, particularly due to an insufficient population of close-to-thermal particles. The hot N_2 and CH_4 populations induced by exothermic chemistry are found to have densities 2 to 3 orders of magnitude smaller than those estimated from INMS data, and escape fluxes more than an order of magnitude smaller than those obtained by estimating the average energy deposition required to produce the hot corona by pick-up ion sputtering (De La Haye et al., 2007). Further investigations are required to justify the INMS exospheric observations. It is proposed that these studies place the focus on sputtering, especially that induced by pick-up ion heating, and on heating by repeated charge exchanges between atmospheric neutrals and magnetospheric or pick-up ions.

Acknowledgments

References

Brecht, S.H., Luhmann, J.G., Larson, D.J., 2000. Simulation of the saturnian magnetospheric interaction with Titan. J. Geophys. Res. 105, 13119–13130.

Burcat, A., 2001. Third millennium ideal gas and condensed phase thermochemical database for combustion. Report 867, Technion Aerospace Engineering.

Chase, M.W., 1998. NIST-JANAF Thermochemical Tables. Fourth ed. J. Phys. Chem. Ref. Monograph 9.

Cravens, T.E., Keller, C.N., Ray, B., 1997. Photochemical sources of non-thermal neutrals for the exosphere of Titan. Planet. Space Sci. 45 (8), 889–896.

Cravens, T.E., Lindgren, C.J., Ledvina, S.A., 1998. A two-dimensional multifluid MHD model of Titan's plasma environment. Planet. Space Sci. 46 (9–10), 1193–1205.

De La Haye, V., Waite Jr., J.H., Johnson, R.E., Yelle, R.V., Cravens, T.E., Luhmann, J.G., Kasprzak, W.T., Gell, D.A., Magee, B., Leblanc, F., Michael, M., Jurac, S., Robertson, I.P., 2007. Cassini INMS data in Titan's upper atmosphere and exosphere: Observation of a suprathermal corona. J. Geophys. Res., doi:10.1029/2006JA012222, in press.

Gan, L., Keller, C.N., Cravens, T.E., 1992. Electrons in the ionosphere of Titan. J. Geophys. Res. 97, 12136–12151.

Hirschfelder, J.O., Curtiss, C.F., Bird, R.B., 1954. The Molecular Theory of Gases and Liquids. Wiley, New York.

Keller, C.N., Cravens, T.E., Gan, L., 1992. A model of the ionosphere of Titan. J. Geophys. Res. 97 (A8), 12117–12135.

Keller, C.N., Anicich, V.G., Cravens, T.E., 1998. Model of Titan's ionosphere with detailed hydrocarbon ion chemistry. Planet. Space Sci. 46 (9/10), 1157–1174.

Lammer, H., Bauer, S.J., 1991. Non-thermal atmospheric escape from Mars and Titan. J. Geophys. Res. 96 (A2), 1819–1825.

Lammer, H., Bauer, S.J., 1993. Atmospheric mass loss from Titan by sputtering. Planet. Space Sci. 41, 657–663.

Lebonnois, S., 2005. Benzene and aerosol production in Titan and Jupiter's atmospheres: A sensitivity study. Planet. Space Sci. 53, 486–497.

Lebonnois, S., Toublanc, D., Hourdin, F., Rannou, P., 2001. Seasonal variations of Titan's atmospheric composition. Icarus 152, 384–406.

Lebonnois, S., Bakes, E.L.O., McKay, C.P., 2003. Atomic and molecular hydrogen budget in Titan's atmosphere. Icarus 161, 474–485.

Lias, S.G., Bartness, J.E., Liebman, J.F., Holmes, J.L., Levin, R.D., Mallard, W.G., 1988. Gas-phase ion and neutral thermochemistry. J. Phys. Chem. Ref. Data 17 (Suppl. 1), 1–861.

Ma, Y.J., Nagy, A.F., Cravens, T.E., Sokolov, I.V., Clark, J., Hansen, K.C., 2004. 3-D global MHD model prediction for the first close flyby of Titan by Cassini. Geophys. Res. Lett. 31, doi:10.1029/2004GL021215. L22803.

McEwan, J.M., Phillips, L.F., 1975. Chemistry of the Atmosphere. Halsted Press Book, New York.

Michael, M., Johnson, R.E., 2005. Energy deposition of pickup ions and heating of Titan's atmosphere. Planet. Space Sci. 53, 263–267.

Michael, M., Johnson, R.E., Leblanc, F., Liu, M., Luhmann, J.G., Shematovich, V.I., 2005. Ejection of nitrogen from Titan's atmosphere by magnetospheric ions and pick-up ions. Icarus 175, 263–267.

Nagy, A.F., Banks, P.M., 1970. Photoelectron fluxes in the ionosphere. J. Geophys. Res. 75 (31), 6260–6270.

Nagy, A.F., Cravens, T.E., 1981. Hot oxygen atoms in the upper atmosphere of Venus. Geophys. Res. Lett. 8 (6), 629–632.

Nagy, A.F., Cravens, T.E., 1988. Hot oxygen atoms in the upper atmosphere of Venus and Mars. Geophys. Res. Lett. 15 (5), 433–435.

Rowley, R.L., Wilding, W.V., Oscarson, J.L., Yang, Y., 2003. Physical and Thermodynamic Properties of Pure Chemicals: Core Edition Plus Supplements 1–13. Taylor & Francis, New York.

Schunk, R.W., Nagy, A.F., 2000. Ionospheres: Physics, Plasma Physics, and Chemistry. Cambridge Univ. Press, Cambridge.

Shematovich, V.I., 1998. Kinetic modeling of suprathermal nitrogen atoms in the Titan's atmosphere. I. Sources. Sol. Syst. Res. 32, 384–391.

Shematovich, V.I., Johnson, R.E., 2006. Hot oxygen coronas at terrestrial planets. In: Proceedings of the European Planetary Science Congress, Berlin, Germany, September 2006. eSPC2006-A-00193.

Shematovich, V.I., Johnson, R.E., Michael, M., Luhmann, J.G., 2003. Nitrogen loss from Titan. J. Geophys. Res. 108 (E8), doi:10.1029/2003JE002094. 5087.

Shematovich, V.I., Tully, C., Johnson, R.E., 2001. Suprathermal nitrogen atoms and molecules in Titan's corona. Adv. Space Res. 27 (11), 1875–1880.

Strobel, D.F., Meier, R.R., Summers, M.E., Strickland, D.J., 1991. Nitrogen airglow sources: Comparison of Triton, Titan and Earth. Geophys. Res. Lett. 18, 689–692.

Vuitton, V., Doussin, J.-F., Benilan, Y., Raulin, F., Gazeau, M.-C., 2006. Experimental and theoretical study of hydrocarbon photochemistry applied to Titan stratosphere. Icarus 185, 287–300.

Vuitton, V., Yelle, R., 2005. Ethane chemistry on Titan. In: Proceedings of the Titan/Cassini-Huygens Meeting, Crete, Greece, May 2005.

Wilson, E.H., Atreya, S.K., 2004. Current state of modeling the photochemistry of Titan's mutually dependent atmosphere and ionosphere. J. Geophys. Res. 109, doi:10.1029/2003JE002181. E06002.